Multiscale Modeling for Surface Composition of Spray-Dried Two-Component Powders

Jie Xiao
School of Chemical and Environmental Engineering, College of Chemistry, Chemical Engineering and Materials Science, Soochow University, Suzhou, Jiangsu Province 215123, P.R. China

Xiao Dong Chen
School of Chemical and Environmental Engineering, College of Chemistry, Chemical Engineering and Materials Science, Soochow University, Suzhou, Jiangsu Province 215123, P.R. China

Dept. of Chemical and Biochemical Engineering, College of Chemistry and Chemical Engineering, Xiamen University, Xiamen 361005, P.R. China

DOI 10.1002/aic.14452
Published online April 3, 2014 in Wiley Online Library (wileyonlinelibrary.com)

Spray drying is a primary process for manufacturing various powder products. One of the most important properties of powders is the ability to get wet. Surface chemical composition critically influences this property. Furthermore, surface composition also influences the efficiency of production as it affects the stickiness of the powder. This work is an attempt to analyze the surface compositions of spray-dried two-component powders produced under various conditions using an innovative multiscale modeling approach. A molecular-level geometrical interpretation is seamlessly coupled with a continuum diffusion model. The predictions are compared with the measurements done on the protein–lactose system using X-ray photoelectron spectroscopy. Sample calculations for the system have demonstrated that the new approach helps reveal surface formation mechanisms much better than that explained with the monoscale continuum approach. This work provides a good basis for a fruitful area of study toward surface composition-focused powder quality control that will have a positive impact in industries. © 2014 American Institute of Chemical Engineers *AIChE J*, 60: 2416–2427, 2014

Keywords: surface composition, spray drying, multiscale modeling, surface formation mechanisms, molecular packing

Introduction

Spray drying is a primary process in food, pharmaceutical, ceramic, polymer, and chemical industries for manufacturing a wide range of powder products.[1] Although the basic technology has been used for over a century, critical processing challenges still exist with regards to powder quality control.[2,3] Since the functionality of a spray-dried powder product usually includes the incorporation efficiency of powder particles into water (i.e., particles' wettability and dissolution behavior), the microstructure and chemical composition of the powder surface (i.e., the powder–water interface) play an indispensable role.[4] On the processing aspect, it is also noted that powder stickiness affects the powder deposition on dryer walls. When powder is too sticky, it may even affect the yield. Consequently, quantitative relationships between the powder surface composition and the feed properties and drying conditions are highly useful for unveiling particle formation and quality maintaining mechanisms.

There has been a consistent stream of experimental efforts devoted to quantitative measurements of the surface composition of lab-scale to industrial-scale spray-dried powders as well as investigations on the relationships of lab conditions to the end-use properties. The well-established technique used in this area is electron spectroscopy for chemical analysis (otherwise known as X-ray photoelectron spectroscopy [XPS]), which can detect around 10-nm deep into the powder surface for chemical compositions.[5,6] Fäldt and Bergenståhl[5,7,8] performed experiments on the (two-component) lactose–casein and (three-component) whey protein–lactose–soybean oil systems. They discovered that the powder surface composition can be quite different from the bulk composition (or the average composition across the dried particle radius) and the surface composition clearly affects the wettability and the dissolution behavior of a particle. Kim et al.[6,9,10] systematically investigated the distribution of milk components in the near surface region of several industrial and lab-scale spray-dried dairy powders, and the changes in the surface composition during long-term storage. The significant difference between surface and bulk compositions was also observed, indicating a kind of solute segregation that must occur during spray drying.

There has been a considerable interest in how drying conditions affect the segregation of different solutes/solids at a

Correspondence concerning this article should be addressed to J. Xiao at jie.xiao@suda.edu.cn or X.D. Chen at xdchen@suda.edu.cn.

droplet surface and hence the powder surface composition.[2,11] The spray drying conditions that have been investigated include feed solids content, drying temperature, initial droplet size, and degree of homogenization.[12–15] The qualitative conclusions on the effects of those drying conditions are, however, arguable and thus difficult in providing quantitative "instructions" to guide the spray drying practice toward controlling the particle surface formation. One major reason for complications is that conventional spray-dried particles usually have a wide size distribution due to the polydispersity of the atomization. It is extremely difficult to correlate a specific particle with the original droplet and precisely track the distinctive drying condition experienced by the specific droplet. Recently, Wu et al.[16] designed a microfluidic-jet-spray dryer that can produce uniform particles by drying monodispersed droplets. Uniform-sized droplets experience similar drying history, which allows a direct correlation of a certain surface composition with a specific drying condition. The notable advantages of this new approach have been demonstrated preliminarily in a few recent studies, where the effects of spray drying temperature and feed solid content on powder structure and property were reported.[3,17]

To better understand the powder formation mechanism and quantitatively relate feed solution composition and processing condition to powder structure and property, tremendous efforts have been made to mathematically model spray drying at different scales. At the macroscale, the system investigated is a complete spray dryer with a certain flow of drying air and spray of droplets. The heat, momentum, and mass conservations have been modeled and solved using computational fluid dynamics techniques. In addition to flow patterns of the gas phase, the models can track the trajectory, residence time, temperature, mass, and moisture content of each droplet.[18–22] However, those models cannot contribute to fundamental understanding of the drying phenomena at individual droplet or particulate level. As a result, during the last decade, growing attention has been given to the theoretical study of spray drying at the single droplet scale.[23] The models based on the characteristic drying rate curve approach and the reaction engineering approach are semi-empirical and can be used to predict the moisture contents of powders.[24] Nevertheless all of these can be categorized as lumped approaches. Within a droplet, the moisture content gradient will inevitably lead to the solute concentration gradient, which implies the diffusion of the solute or suspended solid components. It is understandable that, when multiple solutes/solids are involved, solute/solid segregation may occur during the drying process. These phenomena (i.e., concentration-gradient-driven solute migration) and the other two (i.e., crust formation and surface activity) are considered to be three key mechanisms for the significant difference between the surface composition and the bulk composition of a spray-dried particle.[10–13] Wang and Langrish[25,26] developed a distributed parameter model in an attempt to evaluate the aforementioned mechanisms quantitatively. The model seems to predict the trend of the dryer inlet temperature effect well but the simulated surface concentration is always lower than that estimated based on the XPS measurements.[26] Chen et al.[4] described the onset of solid formation around the outermost layer of a single droplet during the dying process by resorting to an innovative continuum approach starting from the diffusion–convection partial differential equations and using the idea of the characteristic length to reduce the complexity of the equations. With a few derivations, the model system becomes a set of algebraic equations, which can be easily solved to get the surface composition. This approach was adopted to analyze a two-component and a three-component system, respectively, against the XPS data published on dairy fluids.[4,27] Despite the apparent success of the work for three components using the continuum theory,[4] the straight application of the theory to the two-component system did not work. The theoretical estimates for the protein–lactose system were always greater than the XPS measurement results.[27]

For the surface composition, the underprediction by Wang and Langrish[26] and the overprediction by Chen et al.[27] have raised a challenging question about whether the continuum theory alone is sufficient to characterize powder surface formation. As described above, the XPS technique can detect the composition around 10-nm deep into the powder surface.[4] Within such a thin layer, the continuum theory of diffusion is probably not valid as the molecular sizes of certain components (e.g., protein and fat) are larger than 10 nm. Consequently, for the investigation of surface formation, there is an urgent need to develop a novel approach that can link the molecular-level interpretation of solute packing in the thin surface layer with the continuum level description of solute migration through the entire droplet/particle. In this regard, population balance model has shown promise in interrelating mass transport in the droplet with locking point conditions. This method deals with dispersed solute particles as a population and takes into account the change of particle distribution caused by possible aggregation.[28,29] In this work, we have significantly extended the continuum model of Chen et al.[4] by coupling it with a molecular-level geometrical packing model that incorporates a number of scenarios. The multiscale method allows us to project quantitatively the surface compositions of spray-dried two-component particles based on the initial compositions of the original fluids. The comparisons made between the theory and measurements have demonstrated some useful insights of the process. These insights on surface formation mechanisms and potential future research directions are also discussed.

Multiscale Model Development

Macroscale multicomponent diffusion model

Recently, based on the continuum-scale diffusion theory, Chen et al.[4] reported an analytical approach to estimate the surface composition of a spray-dried multicomponent particle. The procedure is summarized briefly first in this section to aid understanding of the current multiscale analysis. Note that our analysis is focused only on the particle surface composition, rather than the composition distribution over the whole cross section of a particle. A multicomponent system is considered but, to simplify the analysis, the components are assumed to be chemically noninteractive to each other. Furthermore, the transport equations for the multicomponent diffusion with mutual diffusivities are not used.[30] Instead, the type of interaction considered is that the components form the dense phase together for solid surface formation, which is reflected by the build up of viscosity. During air drying, the convective mass transfer (along the radial direction r only) in an aqueous droplet can be described mathematically as

$$\frac{\partial c_i}{\partial t} - \xi \frac{dR}{dt}\frac{\partial c_i}{\partial r} \approx \frac{1}{r^2}\frac{\partial}{\partial r}\left(D_{iw} r^2 \frac{\partial c_i}{\partial r}\right) \tag{1}$$

where c_i is the mass concentration of species i (kg/m^3) and D_{iw} the mass diffusivity of species i in solvent w (m^2/s). The

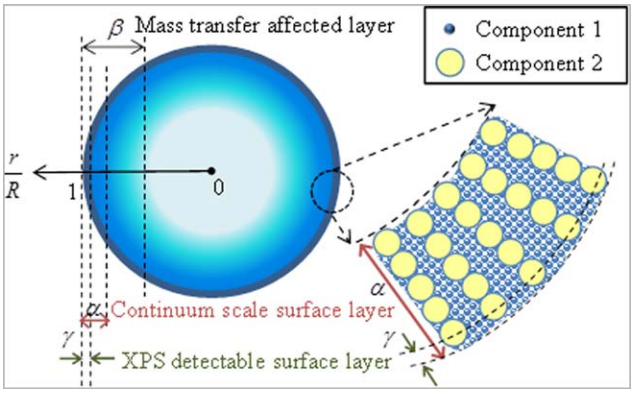

Figure 1. Multiscale illustration of different layers (dimensionless) in a spray-dried two-component particle.

[Color figure can be viewed in the online issue, which is available at wileyonlinelibrary.com.]

radial velocity of solvent is taken as a positive fraction (i.e., ξ) of the shrinking velocity of the droplet surface (i.e., dR/dt). Note that the shrinking velocity is in the negative-r direction. Solvent may not move as such. Eq. 1 assumes that the droplet is dried uniformly at all directions.

Integrating Eq. 1 from $r=0$ to $r=R$, with a zero flux boundary condition at the droplet center and an assumption that the majority of the change in concentration occurs in the mass transfer affected layer with a thickness of βR (see Figure 1), one can obtain

$$\frac{\partial(\bar{c}_i R)}{\partial t} - \xi \frac{dR}{dt}\left(c_{i,s} - c_{i,o}\right) \approx D_{iw,s} \frac{1+2\beta}{\beta R}\left(c_{i,s} - \bar{c}_i\right) \tag{2}$$

The initial concentration (in solution before drying) of species i is denoted as $c_{i,o}$, while within the continuum-scale surface layer (see Figure 1), the species concentration and diffusivity are given by $c_{i,s}$ and $D_{iw,s}$, respectively. The average concentration can be calculated as

$$\bar{c}_i = \frac{m_i}{(4/3)\pi R^3} \approx c_{i,o}(1-\beta) + \frac{c_{i,o}+c_{i,s}}{2}\beta \tag{3}$$

where m_i is the mass of component i in the droplet or dried particle (kg). Substituting Eq. 3 into Eq. 2, and after some manipulations, one obtains

$$\frac{dR}{dt} \approx -D_{iw,s} \frac{1+2\beta}{\beta R} \frac{(1-0.5\beta)\left(c_{i,s} - c_{i,o}\right)}{2c_{i,o} + (\beta+\xi)\left(c_{i,s} - c_{i,o}\right)} \tag{4}$$

Later, it will be shown that β has only a small effect on the predicted results. One modified version of the Stokes–Einstein equation by considering the effect of the solute concentration on fluid viscosity can be used to estimate the diffusion coefficient, which emphasizes the "crowding effect" vigorously[31]

$$D_{iw,s} = f(\phi_s)\frac{k_B T}{6\pi\mu_w R_i} = \left(1 - \frac{\phi_s}{\phi_{max}}\right)^2 \frac{k_B T}{6\pi\mu_w R_i} \tag{5}$$

where μ_w is the viscosity of the pure solvent, R_i the molecular radius of the solute i, ϕ_s the volume fraction of the mixture of all solute species involved in the continuum-scale surface layer, ϕ_{max} the maximum packing volume fraction of all solute species. Note that the function $f(\phi_s)$ approaches unity when ϕ_s approaches zero (i.e., the highly diluted case) and Eq. 5 becomes the standard Stokes–Einstein equation. However, when the surface layer is fully packed by solute molecules or suspended solid particles (i.e., $\phi_s = \phi_{max}$), the surface material becomes highly viscous and the diffusion coefficient would become zero. Replacing the diffusivity in Eq. 4 by the RHS of Eq. 5 yields

$$\frac{dR}{dt} \approx -f(\phi_s)\frac{k_B T}{6\pi\mu_w R_i}\frac{1+2\beta}{\beta R}\frac{(1-0.5\beta)\left(c_{i,s} - c_{i,o}\right)}{2c_{i,o} + (\beta+\xi)\left(c_{i,s} - c_{i,o}\right)} \tag{6}$$

Rearranging the above equation to make the LHS species independent

$$R\frac{dR}{dt}\frac{6\pi\mu_w}{f(\phi_s)k_B T}\frac{\beta}{(1-0.5\beta)(1+2\beta)} \approx -\frac{1}{R_i}\frac{c_{i,s} - c_{i,o}}{2c_{i,o} + (\beta+\xi)\left(c_{i,s} - c_{i,o}\right)} \tag{7}$$

Intuitively, the above equation reflects the fact that all solute species "swim in the same pond" (in the same fluid) and thus for species i and j, we can obtain the ratio

$$1 = \frac{R_j}{R_i}\frac{c_{i,s} - c_{i,o}}{2c_{i,o} + (\beta+\xi)\left(c_{i,s} - c_{i,o}\right)}\frac{2c_{j,o} + (\beta+\xi)\left(c_{j,s} - c_{j,o}\right)}{c_{j,s} - c_{j,o}} \tag{8}$$

This is equivalent to

$$\frac{R_i}{R_j} = \frac{c_{i,s} - c_{i,o}}{c_{j,s} - c_{j,o}}\frac{2c_{j,o} + (\beta+\xi)\left(c_{j,s} - c_{j,o}\right)}{2c_{i,o} + (\beta+\xi)\left(c_{i,s} - c_{i,o}\right)} \tag{9}$$

For a system containing K species, we need to have K independent equations to determine the surface composition, that is, $c_{i,s}$, $i=1,2,\ldots,K$. Eq. 9 provides $K-1$ independent equations, and the other one can be the equation relating the surface layer packing fraction and the surface composition, that is

$$\phi_s = \frac{1}{V_\alpha}\sum_{i=1}^{K}\frac{V_\alpha c_{i,s}}{\rho_i} = \sum_{i=1}^{K}\frac{c_{i,s}}{\rho_i} \tag{10}$$

where V_α is the volume of the continuum-scale surface layer (m^3) (see Figure 1) and ρ_i is the density of species i (kg/m^3). With a given ϕ_s, one can calculate $c_{i,s}$ by solving Eqs. 9 and 10 and further determine the surface coverage (i.e., mass fraction) of species i

$$\omega_{i,\alpha} = V_\alpha c_{i,s}\left(\sum_{j=1}^{K} V_\alpha c_{j,s}\right)^{-1} = c_{i,s}\left(\sum_{j=1}^{K} c_{j,s}\right)^{-1} \quad i=1,2,\ldots,K \tag{11}$$

In the current study, we emphasize that the continuum diffusion model cannot determine the surface packing fraction (ϕ_s), which is related to the detailed molecular packing configurations. An additional molecular-scale packing model is required for calculating surface composition in a more realistic manner. It is noted that the above methodology applies to K number of species. However, to obtain a more definitive description and make better judgment of molecular packing in the surface layer, we will, in the current work, only investigate two-component systems, that is, $K=2$. Extension of this molecular-level approach to $K>2$ will be highly beneficial.

Microscale two-component packing model

As mentioned earlier, we restrict our investigation to a two-component system with Species 1 and 2, whose

molecular sizes are R_1 and R_2 ($R_1 < R_2$), respectively, which is already of practical significance. For example, it was reported that the addition of protein to a lactose solution can alter surface properties of spray-dried powders.[5] Modeling surface compositions for this two-component system could help understand experimental observations and potentially lead to strategies toward controlled particle formation.

To evaluate ϕ_s, we need a microscale level analysis. It is suggested that, intuitively, during spray drying, the capillary force first packs the large particles into an ordered pattern/configuration, while the small particles are still mobile. As drying proceeds, the small particles are gradually packed in the remaining space due to the work of the immersion capillary force. Then, a fairly regular and ordered structure is formed over a relatively longer period of time.[4,32] Correspondingly, a geometric packing model can be rationally developed to provide an additional relationship between the packing fraction ϕ_s and the composition $\omega_{i,\alpha}$ of the continuum-scale surface layer. As shown in Figure 1, this layer ($(1-\alpha)R \le r \le R$) has a characteristic thickness of l_c ($=\alpha R$), which will be referred to as the α layer in the following text. It is further assumed that the large molecules (Species 2) are regularly aligned into N columns in the α layer as shown in Figure 1. The total volume of Species 2 in the α layer is then

$$V_{2,\alpha} = N n_2 \frac{4}{3}\pi R_2^3 \tag{12}$$

where n_2 is the number of Species 2 molecules in each column. Also, the packing fraction of Species 2 in the α layer is

$$\phi_2 = \frac{V_{2,\alpha}}{V_\alpha} \tag{13}$$

The remaining space is packed by Species 1 in some manner to reach a packing fraction of ϕ_1, then the total volume of Species 1 would be

$$V_{1,\alpha} = \left(V_\alpha - V_{2,\alpha}\right)\phi_1 \tag{14}$$

The overall packing fraction is then estimated with

$$\phi_s = \frac{V_{2,\alpha}+V_{1,\alpha}}{V_\alpha} = \phi_2 + (1-\phi_2)\phi_1 = \phi_1 + (1-\phi_1)\phi_2 \tag{15}$$

Since the α layer discussed in this section is essentially the continuum-scale surface layer (Figure 1), the surface coverage data $\omega_{i,\alpha}$ provided by the continuum model can be correlated with packing fractions as

$$\omega_{2,\alpha} = 1-\omega_{1,\alpha} = \frac{V_{2,\alpha}\rho_2}{V_{2,\alpha}\rho_2 + V_{1,\alpha}\rho_1} \tag{16}$$

Substituting Eqs. 13 and 14 to Eq. 16 and rearranging the resulting equation, one obtains

$$\phi_2 = \left(1 + \frac{\rho_2}{\rho_1}\frac{1}{\phi_1}\frac{1-\omega_{2,\alpha}}{\omega_{2,\alpha}}\right)^{-1} \tag{17}$$

Replacing ϕ_2 in Eq. 15 by Eq. 17, one has

$$\phi_s = \phi_1 + (1-\phi_1)\left(1 + \frac{\rho_2}{\rho_1}\frac{1}{\phi_1}\frac{1-\omega_{2,\alpha}}{\omega_{2,\alpha}}\right)^{-1} \tag{18}$$

For a given mass fraction provided by the continuum theory, the overall packing fraction can be determined by Eq. 18 as long as ϕ_1 is specified. Previous work by Chen et al.[27] assumed that ϕ_1 is essentially the maximum packing fraction for perfect uniformly sized spheres. We will show that this approach leads to an overestimation of ϕ_s. It is indeed a challenging task to find the exact value of ϕ_1, which is determined by the external drying condition and the drying rate. It would involve the complex molecular simulation of drying mediated self-assembly of nanoparticles and will be our future endeavor. Nevertheless, it will be shown in the following that we are able to carry out in-depth qualitative analyses using the limiting value of ϕ_1, which can be appropriately assigned. According to Quemada's model,[31] the maximum packing volume fraction of perfect uniformly sized spheres is ϕ'_{max} (i.e., 0.631), which gives the first restriction on ϕ_1

$$\phi_1 \le \phi'_{max} \tag{19}$$

Quemada's model should also be applicable to the packing of Species 2

$$\phi_2 = \left(1 + \frac{\rho_2}{\rho_1}\frac{1}{\phi_1}\frac{1-\omega_{2,\alpha}}{\omega_{2,\alpha}}\right)^{-1} \le \phi'_{max} \tag{20}$$

Rearranging the above equation yields the second restriction on ϕ_1

$$\phi_1 \le \frac{1-\omega_{2,\alpha}}{\omega_{2,\alpha}}\frac{\rho_2}{\rho_1}\left(\frac{1}{\phi'_{max}} - 1\right)^{-1} \tag{21}$$

Moreover, the amount of Species 2 in the α layer should not exceed the total amount of Species 2 in the entire particle of radius R

$$V_{2,\alpha} = V_\alpha \phi_2 \le V_2 \tag{22}$$

The mass fraction of Species 2 in solids is usually specified to prepare spray-dried solutions. It can be written as a function of V_2, that is

$$w_2 = 1 - w_1 = \frac{\rho_2 V_2}{\rho_2 V_2 + \rho_1 V_1} \tag{23}$$

For a spray-dried two-component particle, the maximum packing fraction can be determined by Quemada's model as well[31]

$$\frac{3}{4}\frac{V_1+V_2}{\pi R^3} \le \phi''_{max} \tag{24}$$

where

$$\phi''_{max} = \phi'_{max} + \left(1-\phi'_{max}\right)\phi'_{max} = \phi'_{max}\left(2-\phi'_{max}\right) \tag{25}$$

Combining Eq. 23 with Eq. 24, one can obtain

$$V_2 \le \frac{4}{3}\pi R^3 \phi''_{max}\left(1 + \frac{w_1}{w_2}\frac{\rho_2}{\rho_1}\right)^{-1} \tag{26}$$

Eq. 22 can then be rewritten as

$$V_\alpha \phi_2 \le \frac{4}{3}\pi R^3 \phi''_{max}\left(1 + \frac{w_1}{w_2}\frac{\rho_2}{\rho_1}\right)^{-1} \tag{27}$$

where the volume of the α layer is

$$V_\alpha = \frac{4}{3}\pi R^3\left(1-(1-\alpha)^3\right) \tag{28}$$

Substituting the LHS of Eq. 27 by Eq. 28 and Eq. 17, one should be able to get the third restriction imposed on ϕ_1 as

$$\phi_1 \le \frac{1-\omega_{2,\alpha}}{\omega_{2,\alpha}}\frac{\rho_2}{\rho_1}\left(\frac{1}{\phi''_{\max}}\left(1-(1-\alpha)^3\right)\left(1+\frac{w_1}{w_2}\frac{\rho_2}{\rho_1}\right)-1\right)^{-1} \tag{29}$$

The limiting value of ϕ_1, by considering Eqs. 19, 21, and 29, is thus

$$\begin{cases} \phi_1 = \min\left(\phi'_{\max},\ \dfrac{\omega_{1,\alpha}}{\omega_{2,\alpha}}\dfrac{\rho_2}{\rho_1}\left(\dfrac{1}{\phi'_{\max}}\max\left(1,\ \psi\right)-1\right)^{-1}\right) \\ \psi = \dfrac{1-(1-\alpha)^3}{2-\phi'_{\max}}\left(1+\dfrac{w_1}{w_2}\dfrac{\rho_2}{\rho_1}\right) \end{cases} \tag{30}$$

It is interesting to note that the effects of the initial solid fractions on the particle surface composition can be integrated into the microscale packing model (Eqs. 18 and 30). As indicated by the term ψ in Eq. 30, the feed solution composition could have a significant effect on the surface composition when the solution contains a small amount of Species 2, that is, $w_1 >> w_2$. Also note that the ratio of the α layer thickness to the particle radius, that is, α as shown in Figure 1, may affect surface composition prediction as well (see Eq. 30). Its value has to be appropriately chosen to ensure valid molecular-level and continuum-scale interpretations, which will be discussed in the following Multiscale Coupling section.

Multiscale coupling

The bidirectional coupling between the macroscopic diffusion model and the microscopic packing model is straightforward. The overall packing fraction ϕ_s in the surface layer provided by the geometrical packing model is used in the diffusion model to calculate the surface coverage $\omega_{i,\alpha}$. The surface coverage is adopted in the packing model to generate the packing fraction. Since the same shell layer (i.e., the α layer) is investigated in both macroscopic and microscopic models, its thickness l_c ($=\alpha R$) has to be selected carefully. At macroscale, a sufficiently fine mesh is needed for solving the continuum model so that satisfactory precision of solutions can be guaranteed. For example, the following may be taken

$$\alpha \le \alpha_{\max} \approx 2\% \tag{31}$$

As shown in Figure 1, the shell layer should also be able to cover the columns of large molecules with each column containing a certain number of molecules (e.g., 5 in the figure). Otherwise, the continuum theory will not be valid in this layer. Mathematically, this requirement can be described as

$$\frac{\alpha R}{2R_2} \ge n_{2,\min} \tag{32}$$

which is equivalent to

$$\alpha \ge n_{2,\min}\frac{2R_2}{R} \approx \frac{10R_2}{R} \tag{33}$$

It will be shown later that the choice of α does affect model predictions.

Packing model–based surface composition quantification

It is important to point out that the detectable depth h ($=\gamma R$) of XPS instruments is only about 10 nm. In many cases

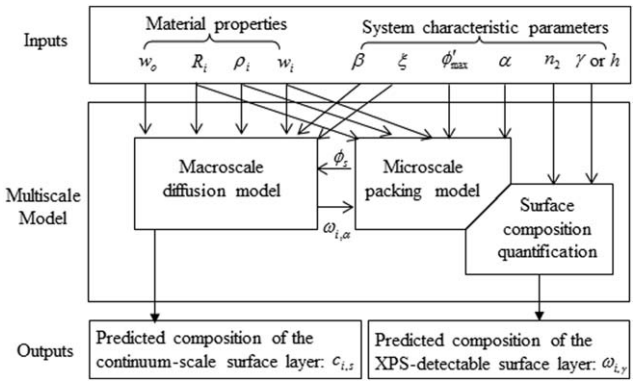

Figure 2. Multiscale model framework and input–output correlations.

$$\frac{h}{2R_2} \ll n_{2,\min} \tag{34}$$

(see the contradiction between Eqs. 32 and Eq. 34) and the XPS detectable layer may contain many partial molecules cut through by the inner surface of this layer (see Figure 1). However, with the detailed packing configurations available, it is feasible to convert the continuum-scale surface coverage to the XPS-detectable surface coverage through a simple geometrical analysis.

Here we use the cases where $h \le R_2$ (Figure 1) to explain this geometrical approach. The number of Species 2 molecular columns can be first derived from Eqs. 12, 13, 17, and 28

$$N = \frac{V_\alpha \phi_2}{n_2 \frac{4}{3}\pi R_2^3} = \frac{R^3\left(1-(1-\alpha)^3\right)}{n_2 R_2^3}\left(1+\frac{\rho_2}{\rho_1}\frac{1}{\phi_1}\frac{1-\omega_{2,\alpha}}{\omega_{2,\alpha}}\right)^{-1} \tag{35}$$

The total volume of spherical caps of Species 2 molecules in the XPS-detectable layer is

$$V_{2,\gamma} \approx N\frac{\pi}{3}h^2(3R_2-h) = N\pi\gamma^2R^3\left(\frac{R_2}{R}-\frac{\gamma}{3}\right) \tag{36}$$

In the same layer, the total volume of Species 1 can be determined as

$$V_{1,\gamma} = \left(V_\gamma - V_{2,\gamma}\right)\phi_1 = \left(\frac{4}{3}\pi R^3\left(1-(1-\gamma)^3\right)-V_{2,\gamma}\right)\phi_1 \tag{37}$$

We can then calculate the XPS-detectable surface coverage as the following

$$\omega_{2,\gamma} = 1-\omega_{1,\gamma} = \frac{V_{2,\gamma}\rho_2}{V_{2,\gamma}\rho_2 + V_{1,\gamma}\rho_1} \tag{38}$$

Solution procedures

Figure 2 shows the model framework and lists the key model inputs and outputs as well as their correlations. The following steps have been summarized for carrying out multiscale analyses of the surface composition of spray-dried two-component particles:

Step1. Solve the macroscopic diffusion model (Eqs. 9 and 10) for an overall packing fraction $\phi_s \in (0,\ 1)$ to get the surface composition $c_{1,s}$ and $c_{2,s}$, which can be further used in Eq. 11 to obtain the surface coverage $\omega_{2,\alpha}$. Repeat this step for different ϕ_s to plot $\omega_{2,\alpha}$ as a function of ϕ_s.

Step 2. Solve the microscopic packing model (Eqs. 18 and 30) for a surface coverage $\omega_{2,\alpha} \in (0,\ 1)$ to get the

overall packing fraction ϕ_s. Repeat this step for different $\omega_{2,\alpha}$ to plot ϕ_s as a function of $\omega_{2,\alpha}$.

Step 3. Plot two curves obtained from both models in one figure and identify their intersection point, which gives the solutions of ϕ_s and $\omega_{2,\alpha}$.

Step 4. Determine the surface composition $\omega_{2,\gamma}$ in the XPS-detectable layer using Eqs. 35–38 for cases described by Eq. 34.

Results and Discussions

In the following section, we investigate the surface composition of spray-dried mixture of lactose–protein (casein), which is a common two-component system in the dairy industry. It has been found experimentally that even with a low concentration of protein (0.01 wt %) in the solution to be dried, protein starts to appear on the surface of the powder. This can significantly reduce the stickiness of the high sugar content products.[33–35] The protein begins to dominate the powder surface composition when the concentration of protein reaches about 1 wt %.[5] The XPS data of the surface composition reported in the same work are used as the benchmark in our current study. Sample calculations are carried out to explore whether it is possible to explain reasonably well this interesting observation. Comparisons are made between predictions by the monoscale model in Chen et al.[4] and the multiscale model developed here to demonstrate the unique capability of the latter approach. The limitations of the current multiscale approach are also discussed to shed light on future developments.

Determination of the model inputs

There are two kinds of inputs need to be specified for surface composition prediction (see Figure 2), that is, materials properties and system characteristic parameters.

Material properties. The approximate molecular sizes of the two species involved in the current analysis (i.e., Species 1: lactose; Species 2: protein) are listed below:

$R_1 \approx 0.62$ nm
$R_2 \approx 25$ nm
Their solid pure densities at 50°C are set as:
$\rho_1 = 1583.6$ kg/m^3
$\rho_2 = 1434$ kg/m^3

These values are directly taken from Chen et al.[4] to be consistent. In the relevant experiments, the lactose solution is mixed with casein (protein) solutions in the following lactose to protein mass proportions: 99.9/0.1, 99/1, 95/5, 80/20, and 60/40, which generates mixture samples with protein mass fractions (i.e., w_2) of 0.1, 1, 5, 20, and 40%, respectively. The solids content w_o of the spray-dried solutions is in all cases 10%. These data are listed in Table 1. Then one can readily calculate initial concentrations of lactose and protein (in solution before drying) as

$$c_{1,o} = \frac{w_o w_1}{\frac{1-w_o}{\rho_{H_2O}} + \frac{w_o w_1}{\rho_1} + \frac{w_o w_2}{\rho_2}} \tag{39}$$

$$c_{2,o} = \frac{w_o w_2}{\frac{1-w_o}{\rho_{H_2O}} + \frac{w_o w_1}{\rho_1} + \frac{w_o w_2}{\rho_2}} \tag{40}$$

System Characteristic Parameters. The mass transfer affected region is assumed to be 25% of the droplet radius, that is, $\beta \approx 0.25$.[36] The radial velocity of solvent is close to the shrinking velocity of the droplet surface, that is, $\xi \approx 1$.[4] According to Quemada's model, the maximum packing volume fraction of perfect uniformly sized spheres ϕ'_{max} is 0.631.[31] As discussed in the Multiscale Coupling section, the ratio of the α layer thickness to the particle radius (i.e., α) can be set to 0.5, 1, 1.5, and 2% in different cases so that its effect on the surface composition can be investigated. At the same time, this shell layer should be able to cover protein columns with each column containing at least five protein molecules, that is, $n_{2,min} = 5$. Moreover, the detectable limit h of the XPS facility used to obtain the laboratory data is about 10 nm.[5]

Sample calculations for Case 1

Macromodel Predictions (Step 1). Given $w_o = 10\%$ and $w_2 = 40\%$, initial concentrations of lactose and protein can be determined using Eqs. 39 and 40

$c_{1,o} = 61.4$ kg/m^3
$c_{2,o} = 40.9$ kg/m^3

For this two-component system, the macroscopic model (Eqs. 9 and 10) becomes

$$\begin{cases} \dfrac{c_{1,s}-c_{1,o}}{c_{2,s}-c_{2,o}} \dfrac{0.75c_{2,o}+1.25c_{2,s}}{0.75c_{1,o}+1.25c_{1,s}} = \dfrac{R_1}{R_2} \approx \dfrac{0.62}{25} = 0.0248 \\ \phi_s = \dfrac{c_{1,s}}{\rho_1} + \dfrac{c_{2,s}}{\rho_2} \end{cases} \tag{41}$$

For different packing fraction ϕ_s ranging from 0 to 1, one can solve the above equation set and obtain a set of $c_{1,s}$ and $c_{2,s}$, which are then used in Eq. 11 to calculate the surface coverage of protein in the continuum-scale surface layer

$$\omega_{2,\alpha} = 1 - \omega_{1,\alpha} = \frac{c_{2,s}}{c_{1,s}+c_{2,s}} \tag{42}$$

The macroscopic model alone offers a quantitative relationship between $\omega_{2,\alpha}$ and ϕ_s, which is shown as a black solid line in Figure 3a. Another line can be obtained if β is set to 0 rather than 0.25, however, it is noted that the difference between two lines can be safely neglected. Thus the choice of β has only a small effect on the predicted results.

Micromodel Predictions (Step 2). When w_2 is 40%, the microscopic packing model (Eqs. 18 and 30) becomes

$$\begin{cases} \phi_s = \phi_1 + (1-\phi_1)\left(1 + 0.906 \dfrac{1}{\phi_1} \dfrac{1-\omega_{2,\alpha}}{\omega_{2,\alpha}}\right)^{-1} \\ \phi_1 = \min\left(0.631,\ 0.906 \dfrac{1-\omega_{2,\alpha}}{\omega_{2,\alpha}} \left(\dfrac{1}{0.631} \max\left(1,\ 1.723\left(1-(1-\alpha)^3\right)\right) - 1\right)^{-1}\right) \end{cases} \tag{43}$$

Table 1. The Laboratory XPS Data on the Solutions Spray Dried with Different Lactose to Protein Ratios (adapted from Fäldt and Bergenståhl)[5]

Case Index	Solids Content (w_o)	Lactose to Protein Mass Ratio (w_1/w_2)	Mass Fraction of Protein in Solids (w_2) (%)	XPS Results on Surface Protein Coverage (wt %)
1	10%	60/40	40	73.4
2		80/20	20	67.4
3		95/5	5	56.7
4		99/1	1	41.7
5		99.9/0.1	0.1	19.7

The quantitative relationship between ϕ_s and $\omega_{2,\alpha}$ obtained from this packing model is plotted in Figure 3a as well (see the thick dashed line). A significant difference between macroscopic and microscopic model outputs can be observed (see the black and blue solid lines and their difference). According to the packing model, as the surface coverage of protein increases, the overall packing fraction initially increases toward ϕ''_{max} and then decreases. As one can anticipate, the maximum packing fraction is smaller than ϕ''_{max}, which is the theoretical maximum for a two-component system. In this special case, the overall packing fraction is always bigger than ϕ'_{max} for any $\omega_{2,\alpha} \in (0, 1)$ (see the vertical dashed lines in Figure 3a). It is interesting to note that α has little effect on the packing model output, since max(1, ψ) is always 1 for any $\alpha \in (0, 0.02]$ when w_2 is 40% (see Figure 4). Thus there is only one thick dashed line in Figure 3a. In later sections, we will show that α can have an impact in other parameter spaces.

Macro-Micro Coupling for Solution Derivation (Step 3). The black line and the blue line intersect at one point, that is, $\left(\phi_s^*, \omega_{2,\alpha}^*\right) = (0.672,\ 0.934)$. This solution gives the overall packing fraction and the protein coverage in the α layer. Since α may influence the relationship between ϕ_s and $\omega_{2,\alpha}$, we further extend the model outputs and plot them in a 3D domain with two surfaces obtained through linear interpolation (see Figure 3b).

Remarks on 2-D–3-D Extension. It should be pointed out that this extension has great importance for understanding the difference between model predictions and experimental data. The third dimension added is α, which is the ratio of the α layer thickness l_c to the droplet radius R. Note that the droplet shrinks during the drying process and R gives the droplet radius when a solid surface is just formed, since we assumed that once a solid layer occurs, negligible further surface composition alternation can happen during the remainder of the drying process.[4] If the number of protein molecules n_2 in one protein column is specified, which means that l_c ($=2n_2R_2$) is determined as well, the investigation on the α effect is essentially a study of the R effect. The solution derived from Figure 3b, that is, the intersection line of two surfaces, gives the overall packing fraction and the protein coverage in the α layer for different-sized droplets. As a result, our model can potentially help to analyze and understand the XPS measurement data for spray-dried powder particles with known size distributions.

Surface Composition Quantification (Step 4). It should be noted that the composition of the XPS-detectable layer (or simply called the γ layer in the following text) depends on several factors (see Eqs. 35–38), including the ratio of the α layer thickness to the droplet radius (i.e., α), the droplet radius (i.e., R), and the XPS detectable depth (i.e., h). When h is fixed at 10 nm, the dependence of $\omega_{2,\gamma}$ on R and α is given in Figure 5. Each line in this figure is obtained by varying n_2 from 5 to 80 for a specified α. Four lines demonstrate the same trend, that is, $\omega_{2,\gamma}$ decreases slightly as the droplet radius increases. This trend is more prominent when α becomes larger. The calculation in this step further confirms that the powder particle-size distribution may need to

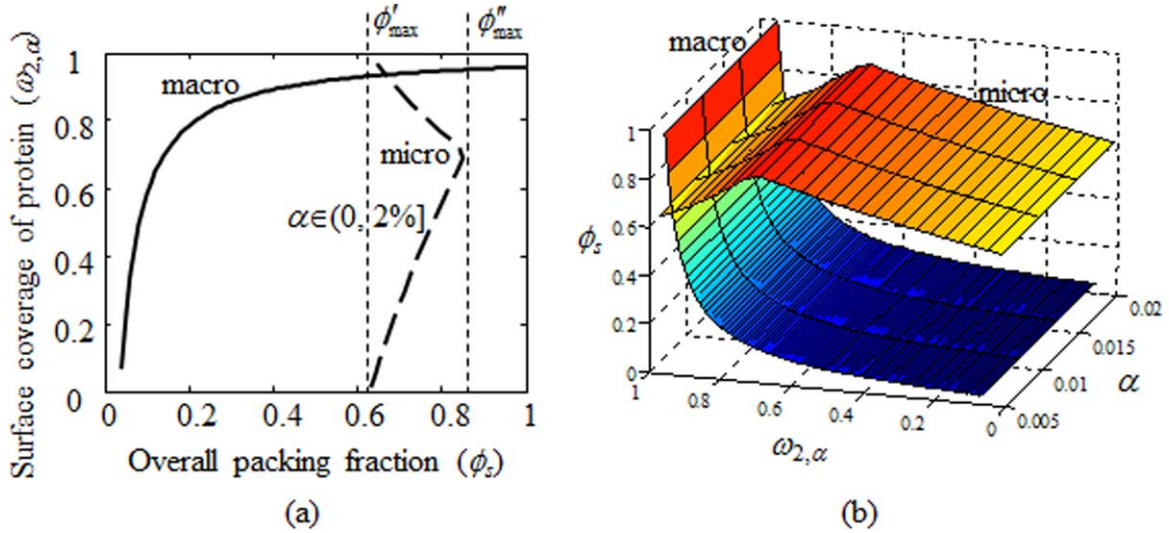

Figure 3. Outputs from macroscopic and microscopic models for the case of $w_o = 10\%$ and $w_2 = 40\%$: (a) a 2-D illustration and (b) a 3-D illustration.

[Color figure can be viewed in the online issue, which is available at wileyonlinelibrary.com.]

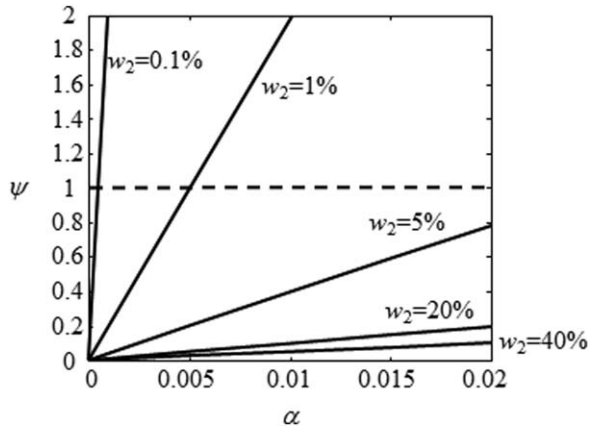

Figure 4. The dependence of ψ on α for different feed solution compositions.

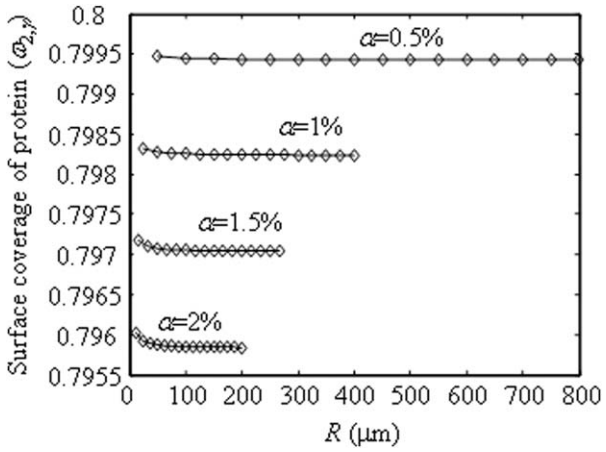

Figure 5. The dependence of the surface coverage of protein in the XPS-detectable layer on the powder particle radius and the ratio of the α layer thickness to the powder radius, when the XPS detectable depth h is 10 nm, w_o is 10% and w_2 is 40%.

be taken into account for XPS data analysis, although the influence of R and α on $\omega_{2,\gamma}$ seems to be negligible in this case (see the range of $\omega_{2,\gamma}$ in Figure 5).

Surface composition prediction for different solution samples

The same procedure presented in the previous section can be applied to Cases 2–5. The predicted 2-D and 3-D results from the macroscopic and microscopic models are given in Figure 6. It is interesting to note that the effect of α on micromodel outputs is significant in Cases 4 and 5 (Figure 6c and d), which is in contrast with Cases 1–3 (Figures 3 and 6a, b). It implies that the surface composition of a spray-dried lactose–protein particle may depend on the droplet size. This dependence may be negligible when the solution to be spray dried contains a large amount of protein, but it becomes significant when the protein content in solution is low (e.g., $w_2 \leq 1\%$). The 3-D plots in Figure 6c, d can provide surface compositions for different-sized droplets. Thus, the multiscale approach introduced in this work could be a powerful tool for rational analysis of XPS data collected from lactose–protein particles with a certain size distribution, especially when particles are spray-dried from low-protein solutions.

Comparison Between Monoscale- and Multiscale-Model Predictions. The protein mass fractions in the α layer (i.e., $\omega_{2,\alpha}$) derived from Figures 3 and 6 for different cases are plotted in Figure 7 (see the red solid line). The results obtained using the monoscale approach in Chen et al.[4] are also given in the same figure for comparison (see the black dashed line). Figure 8 provides the macromodel outputs for all five cases. Chen et al.[4] identified surface compositions by specifying a constant ϕ_s, that is, the solutions are given by the intersection points between the dashed line and the solid lines in Figure 8. Since those solids curves are rather close to each other, especially for Cases 4 and 5, the surface compositions predicted are also very close to each other (see the data points indicated by squares in Figure 7). Comparing model predictions with the XPS data (i.e., the blue line), the multiscale approach clearly outperforms the monoscale approach in capturing the drastic drop in the surface coverage of protein for spray-dried powders when the protein content in solids (w_2) is decreased below ~5 wt %. The identified overprediction (see the difference between the red and blue lines) should be mainly due to the difference between $\omega_{2,\alpha}$ and $\omega_{2,\gamma}$, which are the protein mass fraction in the α layer and that in the γ layer, respectively. The XPS technique can provide the composition data in the γ layer, but not in the α layer (see Figure 1).

Quantification of Surface Compositions. The γ layer compositions calculated using Eqs. 35–38 are shown in Figure 7 (see the green line for $\omega_{2,\gamma}$). It can be seen that the compositions in the γ layer are indeed different from those in the α layer, and they are indeed more relevant to the XPS data. Although the multiscale model predictions cannot perfectly match the XPS results, we have successfully captured the trend in the experimental data qualitatively, especially the low mass fraction end. The existing monoscale methods, however, cannot capture the trend in the experimental data. Consequently, the multiscale model developed in this work holds promise as a powerful tool to explore surface formation mechanisms.

The Lower Bound Solutions. The difference between the model predictions (i.e., the green line) and the experimental data (i.e., the blue line) on surface compositions can be attributed to several reasons. The size distribution of powders spray dried in the laboratory spray dryer used by Fäldt and Bergenståhl[5] has not been taken into account, since the results shown in Figure 7 are obtained with constant n_2 and α, which are set to 5 and 1%, respectively. However, it has been demonstrated that α and n_2 may affect surface compositions significantly, especially for low-protein content solutions (see Figures 5 and 6). In addition, uncertainty exists regarding the XPS detectable depth h. A depth of 10 nm is used in this work, which may not match the experimental facility specifications. It has been observed that the effect of h on $\omega_{2,\gamma}$ cannot be neglected. In Case 1 ($w_2 = 40\%$), for example, if the detection limit is 8 nm rather than 10 nm, the predicted surface composition becomes 75%, which is very close to the measurement value (i.e., 73.4% listed in Table 1). A further analysis of the XPS method will be described in our future work. Furthermore, the assumption of spherical-shaped particles with smooth surfaces may not always be true. Scanning electron microscopy images show that at only 0.1% protein addition (into the lactose solution),

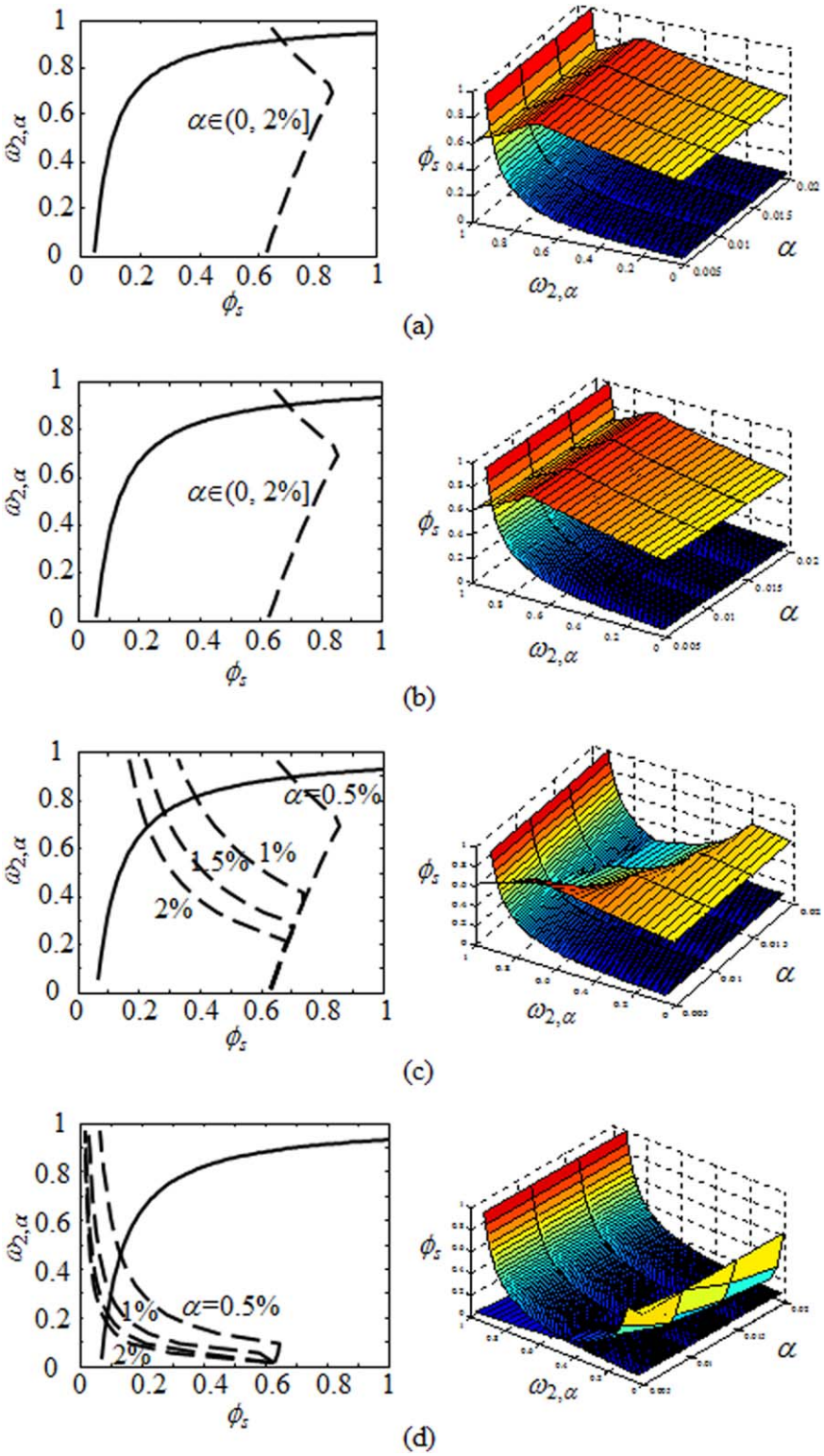

Figure 6. Outputs from macroscopic and microscopic models: (a) Case 2: $w_2 = 20\%$, (b) Case 3: $w_2 = 5\%$, (c) Case 4: $w_2 = 1\%$, and (d) Case 5: $w_2 = 0.1\%$.

[Color figure can be viewed in the online issue, which is available at wileyonlinelibrary.com.]

dents starts to appear at the particle surface.[5] Moreover, the uniform packing of lactose in the α layer shown as Scheme 1 in Figure 9a may not always be valid. It is possible that, the packing fraction of lactose in the γ layer is much higher than the average packing fraction of lactose ϕ_1 in the α layer. When the lactose packing fraction in the γ layer reaches $\phi'_{\max}$ (i.e., Scheme 2 in Figure 9b), the lower bound of $\omega_{2,\gamma}$ can be obtained using Eq. 38 with $V_{1,\gamma}$ calculated as

$$V_{1,\gamma} = (V_\gamma - V_{2,\gamma})\phi'_{\max} = \left(\frac{4}{3}\pi R^3\left(1-(1-\gamma)^3\right) - V_{2,\gamma}\right)\phi'_{\max} \tag{44}$$

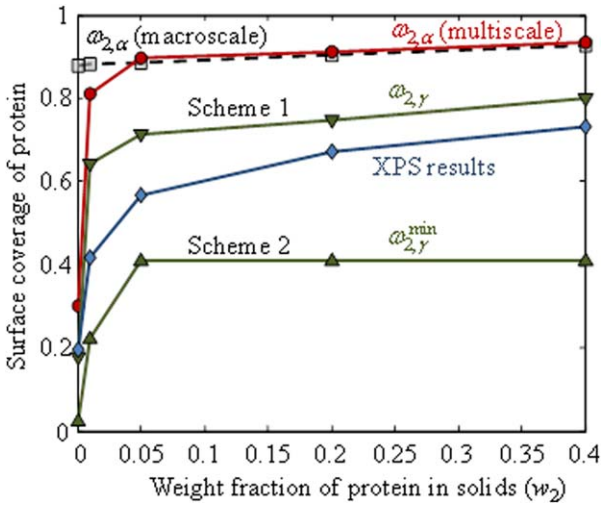

Figure 7. The surface coverage of protein as a function of the initial solution compositions (constant w_o [i.e., 10%] and variant w_2): comparison between the experimental results using XPS analysis by Fäldt and Bergenståhl,[5] theoretically predicted results using the continuum diffusion approach by Chen et al.,[4] and the results predicted by the multiscale approach in this work ($n_2 = 5$, $\alpha = 1\%$, $h = 10$ nm).

[Color figure can be viewed in the online issue, which is available at wileyonlinelibrary.com.]

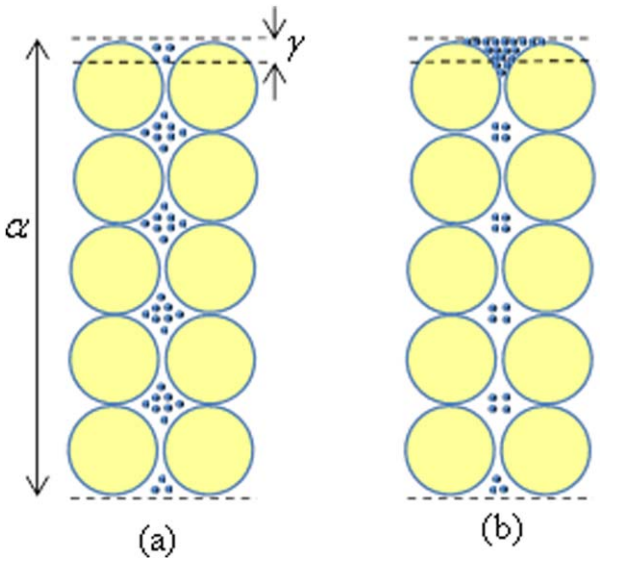

Figure 9. Different packing schemes of lactose in the α layer with the same packing fractions ϕ_1 and ϕ_2: (a) Scheme 1: uniform packing and (b) Scheme 2: surface dominant packing.

The big yellow balls represent protein molecules and the small blue balls denote lactose molecules (not drawn to scale). [Color figure can be viewed in the online issue, which is available at wileyonlinelibrary.com.]

(see the difference between Eqs. 37 and Eq. 44). The solutions are plotted in Figure 7 as well. One can see that $\omega_{2,\gamma}^{min}$ can indeed provide the good lower bound solutions for the XPS results. Also, the averages of $\omega_{2,\gamma}$ and $\omega_{2,\gamma}^{min}$ (i.e., green curves) provide a very good approximation to the XPS data points. The exact packing configuration of components in the surface layer depends on the external drying condition, which will be addressed in our future work.

Further analysis on concentration distributions. It is interesting to compare concentration distributions of lactose and protein within the droplet. The results for Case 1 are shown in Figure 10, where the normalized concentrations are defined as

$$\hat{c}_1 = \frac{c_1}{c_1^{max}} = \frac{c_1}{\rho_1 \phi'_{max}} \tag{45}$$

$$\hat{c}_2 = \frac{c_2}{c_2^{max}} = \frac{c_2}{\rho_2 \phi'_{max}} \tag{46}$$

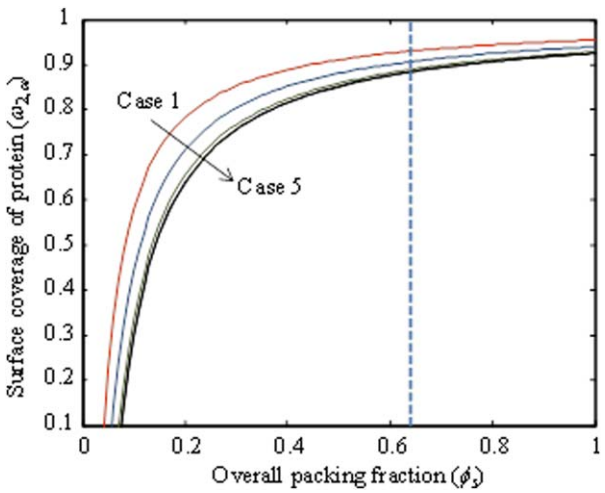

Figure 8. Illustration of solution derivation from the monoscale model (i.e., the macroscopic approach in Chen et al.[4]).

[Color figure can be viewed in the online issue, which is available at wileyonlinelibrary.com.]

For both protein and lactose, the mass concentration gradient is well established within the mass transfer affected region. Along the radial direction, a continuous increase of the lactose concentration from location $(1-\beta)R$ to location R can be observed, that is, $\hat{c}_{1,o} < \hat{c}_{1,s} < \hat{c}_{1,\gamma}$. However, along the same direction, a drastic increase of the protein concentration from $\hat{c}_{2,o}$ to $\hat{c}_{2,s}$ is followed by a concentration drop from $\hat{c}_{2,s}$ to $\hat{c}_{2,\gamma}$. The two distributions seem to contradict each other, but this observation can be understood if we link molecular-level interpretation with the continuum theory. The XPS detectable region, that is, the γ layer of 10 nm in depth, would be able to contain about eight lactose molecules closely lined up in the direction of the depth. It would only, however, contain a thin spherical cap of the protein molecule (see Figure 1). As a result, the continuum diffusion theory is not applicable to the distribution of protein caps in the γ layer and strictly speaking, $\hat{c}_{2,\gamma}$ is not the protein concentration, but the protein cap concentration.

The lactose and protein concentrations in initial solutions and at droplet surfaces for all five cases are compared in Figure 11. Even with a low concentration of protein ($w_2 = 0.1$ wt %) in the solution to be dried, normalized surface concentration of protein (i.e., $\hat{c}_{2,\alpha}$) can reach 5%. Increasing the protein content in the solution from 0.1 to 5 wt %, a drastic increase of $\hat{c}_{2,\alpha}$ from 5 to 100% can be observed in Figure 11b, which implies that the maximum

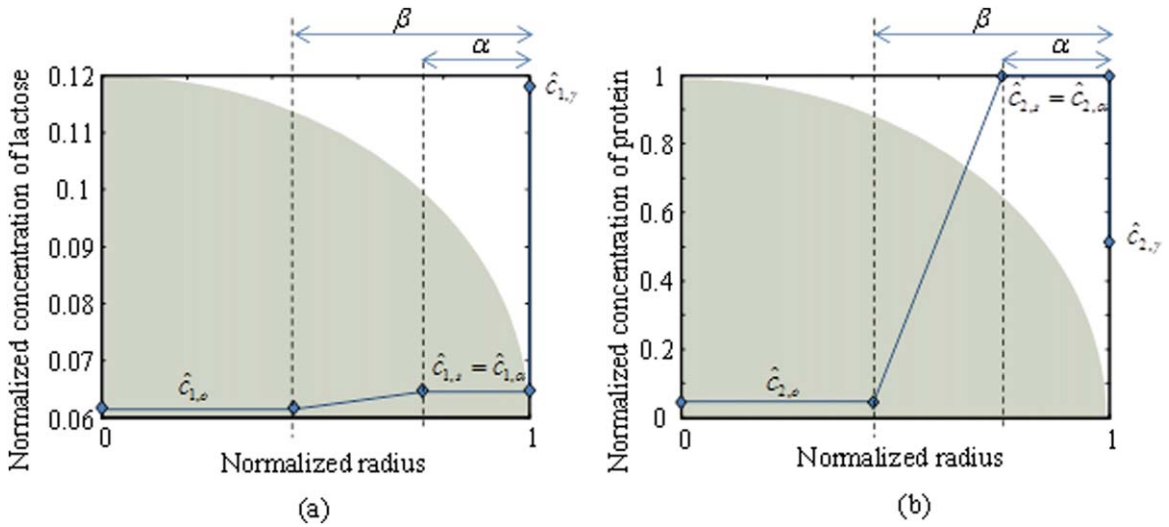

Figure 10. Distributions of normalized concentrations of lactose (a) and protein (b) in a droplet undergoing drying for Case 1.

α and β have been intentionally enlarged to show the topology of the curves. [Color figure can be viewed in the online issue, which is available at wileyonlinelibrary.com.]

packing is achieved for protein in the α layer (see Eq. 46). Thus, $\hat{c}_{2,\alpha}$ keeps unchanged when w_2 is further increased.

It is anticipated that, on the contrary, the normalized surface concentration of lactose (i.e., $\hat{c}_{1,\gamma}$) decreases as the protein content in the solution increases (see the dashed blue line in Figure 11a). In two extreme cases, $\hat{c}_{1,\gamma}$ should be around 100% when the solution contains pure lactose (i.e., $w_2 = 0$ wt %) and it has to be zero when we use pure protein solutions. However, either $\hat{c}_{1,\gamma}$ or $\hat{c}_{1,\gamma}^{\max}$ calculated based on, respectively, the lactose packing Scheme 1 and Scheme 2 (Figure 9), cannot capture the above described trend (see the two green lines and their comparisons with the dashed blue line). This observation implies that the lactose packing depends on the initial solution composition. A transition from surface dominant packing (Scheme 2) to uniform packing (Scheme 1) may exist when the protein content w_2 is increased from 0 to 1 and the transition zone is located around the point where w_2 is close to 5 wt %.

Conclusions

In the current work, a microscopic geometric packing model is seamlessly coupled with a continuum diffusion model preliminarily developed by Chen et al.[4] to describe the solute segregation that occurs during solid surface formation of the spray drying process. Sample calculations for the lactose–protein two-component system demonstrate that the integrated multiscale framework actually works quite well in terms of bridging quantitatively the composition result in the thick continuum-scale surface layer and that in the thin layer detected by the XPS instrument. The effect of protein addition into the lactose solution on the powder surface composition observed in experiments can be fully captured including the very low end of the protein bulk concentrations, which cannot be achieved by the macroscale diffusion model alone. Most importantly, the multiscale model based analysis can help understand the underlying mechanisms of this effect and some insights into the molecular packing schemes have

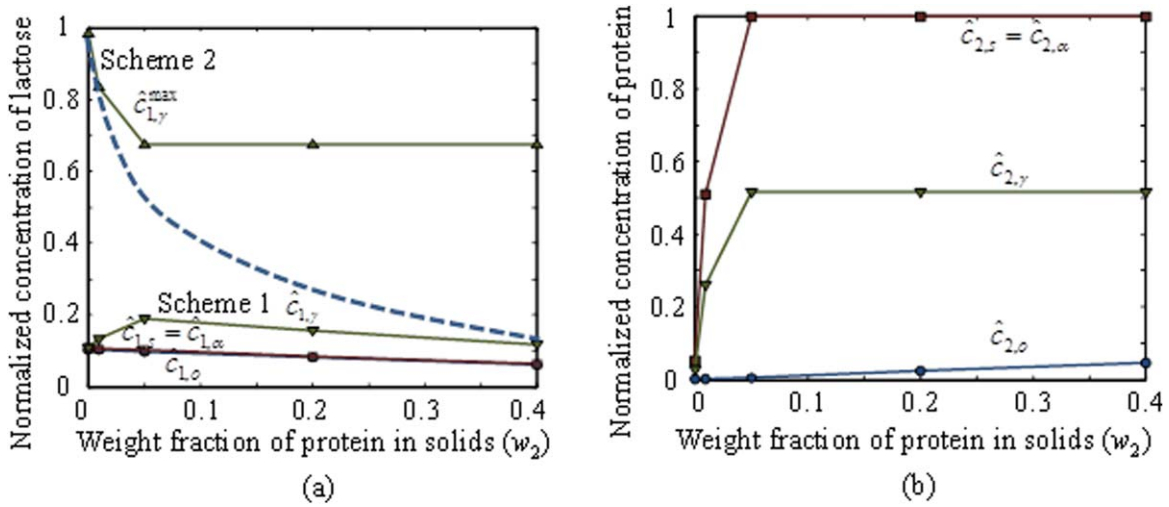

Figure 11. Normalized concentrations of lactose (a) and protein (b) in the initial solution, the α layer and the γ layer as a function of the initial protein content.

[Color figure can be viewed in the online issue, which is available at wileyonlinelibrary.com.]

been generated. Moreover, the model is generic and allows the investigation of the effects of various spray drying conditions and system characteristic parameters on the surface composition of spray-dried two-component powders. In addition to the feed solution composition studied in this work, other parameters that can be thoroughly investigated include the feed solid content, droplet size, and XPS detectable depth, and so forth. The results will be reported in an upcoming article.

The current multiscale approach, however, has disadvantages, as it is restricted to the study of two-component systems and the complex phenomenon of molecular packing for surface formation has not been taken into account. We are now developing a microscopic Monte Carlo based model that can characterize the evaporation induced self-assembly of more than two types of solutes so that a clear picture of 3-D structures formed on the surface can be provided. All these efforts will help tremendously in practice on how to create desirable surfaces, and eventually lead to better powder functionalities and efficient operations of spray drying and other evaporation induced self-assembly processes.

Acknowledgments

This work is supported by the research funds from the National High-tech R&D Program (863 Program, No. 2011AA100802-3) and the "Jiangsu Specially-Appointed Professors Program" of China, and the Youth Fund of Natural Science Foundation of Jiangsu Province of China (No. BK20130293), as well as the Faculty Start-up Funds from Soochow University.

Literature Cited

1. Masters K. *Spray Drying—An Introduction to Principles, Operational Practice and Applications*. London: Leonard Hill Books, 1972.
2. Vehring R, Foss WR, Lechuga-Ballesteros D. Particle formation in spray drying. *Aerosol Sci*. 2007;38:728–746.
3. Wu WD, Liu W, Gengenbach T, Woo MW, Selomulya C, Chen XD, Weeks M. Towards spray drying of high solids dairy liquid: effects of feed solid content on particle structure and functionality. *J Food Eng*. 2014;123:130–135.
4. Chen XD, Sidhu H, Nelson M. Theoretical probing of the phenomenon of the formation of the outermost surface layer of a multicomponent particle, and the surface chemical composition after the rapid removal of water in spray drying. *Chem Eng Sci*. 2011;66:6375–6384.
5. Fäldt P, Bergenståhl B. The surface composition of spray-dried protein-lactose powders. *Colloids Surf A*. 1994;90:183–190.
6. Kim EHJ, Chen XD, Pearce D. On the mechanisms of surface formation and the surface compositions of industrial milk powders. *Drying Technol*. 2003;21:265–278.
7. Fäldt P, Bergenståhl B. Spray-dried whey protein/lactose/soybean oil emulsions. 1. Surface composition and particle structure. *Food Hydrocolloids*. 1996;10:421–429.
8. Fäldt P, Bergenståhl B. Spray-dried whey protein/lactose/soybean oil emulsions. 2. Redispersability, wettability and particle structure. *Food Hydrocolloids*. 1996;10:431–439.
9. Kim EHJ, Chen XD, Pearce D. Surface characterization of four industrial spray-dried dairy powders in relation to chemical composition, structure and wetting property. *Colloids Surf B Biointerfaces*. 2002;26:197–212.
10. Kim EHJ, Chen XD, Pearce D. Surface composition of industrial spray-dried milk powders. 3. Changes in the surface composition during long-term storage. *J Food Eng*. 2009;94:182–191.
11. Wang S, Langrish TAG. A review of process simulations and the use of additives in spray drying. *Food Res Int*. 2009;42:13–25.
12. Kim EHJ, Chen XD, Pearce D. Surface composition of industrial spray-dried milk powders. 1. Development of surface composition during manufacture. *J Food Eng*. 2009;94:163–168.
13. Kim EHJ, Chen XD, Pearce D. Surface composition of industrial spray-dried milk powders. 2. Effects of spray-drying conditions on the surface composition. *J Food Eng*. 2009;94:169–181.
14. Gaiani C, Morand M, Sanchez C, Tehrany EA, Jacquot M, Schuck P, Jeantet R, Scher J. How surface composition of high milk proteins powders is influenced by spray-drying temperature. *Colloids Surf B Biointerfaces*. 2010;75:377–384.
15. Jones JR, Prime D, Leaper MC, Richardson DJ, Rielly CD, Stapley AGF. Effect of processing variables and bulk composition on the surface composition of spray dried powders of a model food system. *J Food Eng*. 2013;118:19–30.
16. Wu WD, Lin SX, Chen XD. Monodisperse droplet formation through a continuous jet break-up using glass nozzles operated with piezoelectric pulsation. *AIChE J*. 2011;57:1386–1392.
17. Rogers S, Wu WD, Lin SXQ, Chen XD. Particle shrinkage and morphology of milk powder made with a monodisperse spray dryer. *Biochem Eng J*. 2012;62:92–100.
18. Jin Y, Chen XD. A three-dimensional numerical study of the gas/particle interactions in an industrial-scale spray dryer for milk powder production. *Drying Technol*. 2009;27:1018–1027.
19. Jin Y, Chen XD. A fundamental model of particle deposition incorporated in CFD simulations of an industrial milk spray dryer. *Drying Technol*. 2010;28:960–971.
20. Jin Y, Chen XD. Entropy production during the drying process of milk droplets in an industrial spray dryer. *Int J Therm Sci*. 2011;50:615–625.
21. Mezhericher M, Levy A, Borde I. Modeling of droplet drying in spray chambers using 2D and 3D computational fluid dynamics. *Drying Technol*. 2009;27:359–370.
22. Mezhericher M, Levy A, Borde I. Three-dimensional spray-drying model based on comprehensive formulation of drying kinetics. *Drying Technol*. 2012;30:1256–1273.
23. Mezhericher M, Levy A, Borde I. Theoretical models of single droplet drying kinetics: a review. *Drying Technol*. 2010;28:278–293.
24. Chen XD, Lin SXQ. Air drying of milk droplet under constant and time-dependent conditions. *AIChE J*. 2005;51:1790–1798.
25. Wang S, Langrish TAG. A distributed parameter model for particles in the spray drying process. *Adv Powder Technol*. 2009;20:220–226.
26. Wang S, Langrish TGA. A multi-component distributed parameter model for spray drying. *7th Asia-Pacific Drying Conference (ADC 2011)*. Tianjin, P.R. China, 2011.
27. Chen XD, Sidhu H, Nelson M. On the addition of protein (casein) to aqueous lactose as a drying aid in spray drying—theoretical surface composition. *Drying Technol*. 2013;31:1–9.
28. Buck A, Peglow M, Naumann M, Tsotsas E. Population balance model for drying of droplets containing aggregating nanoparticles. *AIChE J*. 2012;58:3318–3328.
29. Mezhericher M, Naumann M, Peglow M, Levy A, Tsotsas E, Borde I. Continuous species transport and population balance models for first drying stage of nanosuspension droplets. *Chem Eng J*. 2012;210:120–135.
30. Hecht JP, King CJ. Spray drying: influence of developing drop morphology on drying rates and retention of volatile substances. *2. Modeling. Ind Eng Chem Res*. 2000;39:1766–1774.
31. Quemada D. Lecture notes in physics: stability of thermodynamic systems. In: Cases-Vasquez J, Lebon J, editors. Berlin: Springer, 1982:210.
32. Wang L, Wan Y, Li Y, Cai Z, Li H, Zhao XS, Lin Q. Binary colloidal crystals fabricated with a horizontal deposition method. *Langmuir*. 2009;25:6753–6759.
33. Adhikari B, Howes T, Bhandari BR, Truong V. Stickiness in foods: a review of mechanisms and test methods. *Int J Food Properties*. 2001;4:1–33.
34. Adhikari B, Howes T, Bhandari BR, Troung V. Surface stickiness of drops of carbohydrate and organic acid solutions during convective drying: experiments and modeling. *Drying Technol*. 2003;21:839–873.
35. Adhikari B, Howes T, Lecomte D, Bhandari BR. A glass transition temperature approach for the prediction of the surface stickiness of a drying droplet during spray drying. *Powder Technol*. 2005;149:168–179.
36. Van der Sman RGM. Simple model for estimating heat and mass transfer in regular-shaped foods. *J Food Eng*. 2003;60:383–390.

Manuscript received Sept. 4, 2013, and revision received Feb. 6, 2014.